Four-view Geometry with Unknown Radial Distortion

Supplementary Material

Petr Hruby, Viktor Korotynskiy, Timothy Duff, Luke Oeding, Marc Pollefeys, Tomas Pajdla, Viktor Larsson

Here we give additional details for the main paper P. Hruby, V. Korotynskiy, T. Duff, L. Oeding, M. Pollefeys, T. Pajdla, V. Larsson. *Four-view Geometry with Unknown Radial Distortion*. CVPR 2023.

Our paper combines different areas of expertise within computer vision with algebraic geometry. Hence, here we try to provide more details in order to give a complete picture for both communities.

First, we present more details about the theory with the aim of making an informal explanation of some less familiar concepts from algebraic geometry for computer vision researchers. However, we still want to provide sufficient detail to allow an expert algebraic geometer to check the correctness of our results.

Secondly, we present additional results from the experiments in the main paper. We also present more qualitative examples of real reconstructions from the radial camera reconstruction pipeline, showing that our approach works for general 3D scenes.

7.1. Camera standard forms

Here we provide more details on our camera parameterization and a justification of our choices.

Proposition 2. Let $P_1, \ldots, P_4 \in \mathbb{P}(\mathbb{R}^{2 \times 4})$ be generic. Then there exists $H \in \mathrm{PGL}_4(\mathbb{R})$ such that the transformed cameras $(P_1 H, \ldots, P_4 H)$ have the form in (5).

Proof. Fixing a representation of each camera in homogeneous coordinates, consider the 4×4 matrix obtained by stacking the first row of each camera:

$$A = \begin{bmatrix} P_1[1, :] \\ P_2[1, :] \\ P_3[1, :] \\ P_4[1, :] \end{bmatrix}.$$

For each $i = 1, \ldots 4$, let d_i be the determinant of the matrix obtained by substituting the normalized row vector $(1/P_1[1,1]) \, P_1[2, :]$ for $P_i[1, :]$ in A. Let us set

$$H = (\mathrm{diag}\,(d_1, d_2, d_3, d_4)\, A)^{-1}. \tag{18}$$

This gives a well-defined element of $\mathrm{PGL}_4(\mathbb{R})$, since rescaling any P_i also rescales Eq. (18). To see that the

transformed cameras have the desired form, note first that $(P_i H)[1, :] = d_i^{-1} e_i \sim e_i$ for each $i = 1, \ldots, 4$. Moreover, if $\mathbf{d}$ is a 1×4 vector with $\mathbf{d}\, A = P_1[2, :]$, then by Cramer's rule, $\mathbf{d} \sim \begin{bmatrix} d_1 & d_2 & d_3 & d_4 \end{bmatrix}$, which gives $(P_1 H)[2, :] \sim e_1 + e_2 + e_3 + e_4$. $\square$

Proposition 3. Let $P_1, \ldots, P_4$ be generic calibrated radial cameras. Then there exists a three-dimensional similarity transformation $H \in \mathrm{S}(3)$ such that $(P_1 H, \ldots, P_4 H)$ has the form in (10). Moreover, if each P_i is upright as in (14), then H can be chosen so that $P_i H$ is also upright.

Proof. Consider four arbitrary calibrated radial cameras:

$$P_1 = \begin{bmatrix} \mathbf{r}_{11}^\top & t_{11} \\ \mathbf{r}_{12}^\top & t_{12} \end{bmatrix}, \quad P_2 = \begin{bmatrix} \mathbf{r}_{21}^\top & t_{21} \\ \mathbf{r}_{22}^\top & t_{22} \end{bmatrix},$$

$$P_3 = \begin{bmatrix} \mathbf{r}_{31}^\top & t_{31} \\ \mathbf{r}_{32}^\top & t_{32} \end{bmatrix}, \quad P_4 = \begin{bmatrix} \mathbf{r}_{41}^\top & t_{41} \\ \mathbf{r}_{42}^\top & t_{42} \end{bmatrix}.$$

To fix the first camera, we first transform the cameras by

$$H_1 = \begin{bmatrix} \mathbf{R}_1 & -\mathbf{R}_1 \mathbf{t}_1 \\ \mathbf{0}^\top & 1 \end{bmatrix} \in \mathrm{S}(3),$$

where

$$\mathbf{R}_1 = \begin{bmatrix} \mathbf{r}_{11} & | & \mathbf{r}_{12} & | & \mathbf{r}_{11} \times \mathbf{r}_{12} \end{bmatrix}, \quad \mathbf{t}_1 = \begin{bmatrix} t_{11} \\ t_{12} \\ 0 \end{bmatrix}$$

Then we have

$$\tilde{P}_1 = P_1 H_1 = \begin{bmatrix} 1 & 0 & 0 & 0 \\ 0 & 1 & 0 & 0 \end{bmatrix}$$

To fix the second camera, consider the subgroup of $\mathrm{S}(3)$ that stabilizes $\tilde{P}_1$. Its elements have the form

$$\begin{bmatrix} 1 & 0 & 0 & 0 \\ 0 & 1 & 0 & 0 \\ 0 & 0 & 1 & a \\ 0 & 0 & 0 & b \end{bmatrix}, \quad a, b \in \mathbb{R}, b \neq 0.$$

If we denote the second H_1-transformed camera by

$$\tilde{P}_2 = P_2 H_1 = \begin{bmatrix} \tilde{\mathbf{r}}_{21}^\top & \tilde{t}_{21} \\ \tilde{\mathbf{r}}_{22}^\top & \tilde{t}_{22} \end{bmatrix},$$

we may obtain the form in (10) by choosing a, b such that

$$\tilde{P}_2[:, 3:4] \begin{bmatrix} a \\ b \end{bmatrix} = \begin{bmatrix} 0 \\ 1 \end{bmatrix} \Rightarrow$$

$$\begin{bmatrix} a \\ b \end{bmatrix} = \frac{1}{\det \tilde{P}_2[:, 3:4]} \begin{bmatrix} -\tilde{t}_{21} \\ \tilde{t}_{22} \end{bmatrix}.$$

Notice that in both, the general calibrated and upright cases, this formula gives $b \neq 0$. Thus, setting

$$H_2 = \begin{bmatrix} 1 & 0 & 0 & 0 \\ 0 & 1 & 0 & 0 \\ 0 & 0 & 1 & a \\ 0 & 0 & 0 & b \end{bmatrix}, \quad H = H_1 H_2,$$

we obtain $(P_1 H, \ldots, P_4 H)$ as in Eqs. (10) and (14). $\quad\square$

7.2. Symmetries and Galois groups

In this section, we review some basics of group theory and Galois theory and the way it can be used to discover symmetries in polynomial systems that can be used to decompose large systems into sequences of smaller ones. We also provide additional technical details on symmetries of our polynomial systems.

To understand the relationships between the various formulations of the 13 point problem, note first that

$$3584 = 16 \cdot 224 = 16 \cdot 4 \cdot 56 = 16 \cdot 4 \cdot 2 \cdot 28.$$

Suppose we are given 13 suitably generic $\mathbb{P}^1$ point correspondences. Then, over the complex numbers, there are 28 radial quadrifocal tensors satisfying (4). The symmetry (6) shows that each tensor determines 2 distinct $\mathrm{PGL}_4(\mathbb{R}^{4\times4})$-orbits of camera 4-tuples $(P_1, \ldots, P_4)$. Each set of cameras can be calibrated in 4 different ways (Proposition 1), and SM Propositions 3 and 4 show that the resulting Euclidean reconstructions can be brought to the form (10) in 16 different ways. This decomposition into subproblems is reflected in the structure of the *Galois groups* associated to the various problem formulations. These Galois groups can be *heuristically* computed with numerical HC methods—see eg. [21] for details. We catalogue our results in Table 3, most of which we verified with two separate software systems, `Macaulay2` [30] and `HomotopyContinuation.jl` [9]. We represent the Galois groups using semidirect products. E.g., for the Galois group G_{224} of the formulation with 224 solutions we consider the action map α defined by the action on 56 blocks of size 4 that are preserved by G_{224}. Then, G_{224} is isomorphic to the semidirect product of $K = \ker \alpha$ and $\mathrm{im}\,\alpha \cong G_{56}$. Every permutation from the kernel stabilizes each of 56 blocks. All the blocks can be divided into 28 pairs, where the action of K on every pair is isomorphic to $(S_2 \times S_2) \rtimes S_4$ and the solutions from all the pairs are permuted independently by K. Thus, $K \cong ((S_2 \times S_2) \rtimes S_4)^{28}$. The subgroups $G_{28} = S_{28}, G_{25} = S_{25}, G_{50} = S_2 \wr S_{25}$ obey the principle of being "as large as possible given the observed structure" [74]. Thus, conditional on HC producing a correct set of permutations, we can say each of these three is the full Galois/monodromy group.

We recall the basic "building blocks" that appear in each of the groups. The symmetric group on n letters, denoted S_n, consists of all $n!$ permutations of the set $[n] := \{1, \ldots, n\}$. The alternating group A_n is the set of all $n!/2$ permutations $\sigma \in S_n$ that have an even number of ordered pairs $1 \leq i < j \leq n$ with $\sigma(i) > \sigma(j)$.

We also have combinations of these groups via direct (cartesian) products $\times$, wreath products $\wr$ and semi-direct products $\rtimes$. The *direct product* is the cartesian product of sets with component-wise group multiplication.

The *semi-direct* product of groups gives a way to consider both groups inside a larger group where the product is not necessarily the component-wise product, and hence the products between elements from the components is not necessarily commutative. Typically if N and H are both subgroups of G, with N a normal subgroup, $G = NH$ and $N \cap H = \{e\}$, then we write $G = N \rtimes H$. In this case it is no loss to think of $N \rtimes H$ as the set $\{nh \mid n \in N, h \in H\}$, and one checks that the group product (concatenation) is actually closed. Moreover this (internal) semi-direct product is unambiguous precisely because we have embedded our component groups N, H into another group G. Consequently, in settings like ours where we know how each of the component groups acts on a common set (being part of the Galois group) the action gives the embedding into a larger group, and disambiguates the notation which would otherwise be more complicated since the external semi-direct product is not unique. Also note that $G = NH$ and $N \cap H = \{e\}$ is true both for $G = N \times H$ (both N and H normal in G) and $G = N \rtimes H$ (only assume N normal in G), so for finite groups $|N \times H| = |N \rtimes H|$.

The *wreath product* of symmetric groups $S_n \wr S_m$ can be realized as a semidirect product $\underbrace{(S_n \times \cdots \times S_n)}_{m \text{ times}} \rtimes S_m$. More concretely, it is the group of all $(n!)^m \cdot m!$ permutations of the set $[n] \times [m]$ which preserve the partition of this set into blocks of size n given by $B_i = [n] \times \{i\}$ for $i = 1, \ldots, m$. Roughly speaking, an algebraic problem with nm solutions decomposes as solving a problem with m solutions and then m problems with n solutions if and only if the Galois group of that problem is a subgroup of $S_n \wr S_m$. See eg. [21, Prop. 2.8]. Thus, numerically computing the Galois groups gives a general test for testing the decomposability of minimal problems.

Importantly, each of the (putative) Galois groups from the 13 point problem contains the full symmetric group S_{28}, which acts on the blocks of solutions corresponding to distinct quadrifocal tensors. This implies (see eg. [57]) that an exact solution to the any of these problems cannot be achieved solely by the standard arithmetic operations and extracting roots of polynomials of degree 27 or lower. Thus, in a very precise sense, the number **28** captures the algebraic complexity of these minimal problems. Similarly, our

results indicate that **25** is the algebraic complexity in the upright case.

We now describe the symmetry group for the calibrated formulation. As an abstract group, this is isomorphic to

$$\mathbb{Z}_2 \times \mathbb{Z}_2 \times \mathbb{Z}_2 \times \mathbb{Z}_2.$$

This symmetry group may be understood as a group of deck transformations acting on the fibers of a branched cover associated to the minimal problem [21]. This group is also isomorphic to the Weyl group of the Lie group $(\mathrm{SL}_2)^4$ of symmetries of the variety of principal minors (radial quadrifocal tensors) living in $\mathbb{R}^2 \otimes \mathbb{R}^2 \otimes \mathbb{R}^2 \otimes \mathbb{R}^2$.(cf. [39, § 6].) It can be described by 4 mutually independent generators, which we now describe. The first generator, the "third-column flip" $\Psi_1 : \mathbb{R}^{13} \dashrightarrow \mathbb{R}^{13}$, may be defined in Cayley parameters by

$$\Psi_1(x_2, x_3, x_4, y_2, y_3, y_4, z_2, z_3, z_4, \mathbf{t}_3, \mathbf{t}_4)$$
$$= (-x_2, -x_3, -x_4, -y_2, -y_3, -y_4, z_2, z_3, z_4, \mathbf{t}_3, \mathbf{t}_4). \tag{19}$$

As the name suggests, and can be easily verified using the definition of Cay, this symmetry effects the non-fixed camera matrices (P_2, P_3, P_4) by reversing the sign of the third column in each matrix and leaving all other entries unchanged. Thus, two Ψ_1-conjugate camera matrices are S(3)-equivalent via the matrix

$$H_1 = \mathrm{diag}(-1, -1, 1, -1) \sim \mathrm{diag}(1, 1, -1, 1). \tag{20}$$

For $j = 2, 3, 4$, we may define three more independent symmetries, with formulas analogous to those discussed in [45][Sec. 5.2]. As in the case of Ψ_1, each symmetries has the effect of multiplying all four cameras on the right by some $H_i \in \mathrm{S}(3)$. For $j = 2$,

$$\Psi_2(x_2, x_3, x_4, y_2, y_3, y_4, z_2, z_3, z_4, \mathbf{t}_3, \mathbf{t}_4)$$
$$= \left(\frac{y_2}{z_2}, x_3, x_4, \frac{-x_2}{z_2}, y_3, y_4, \frac{-1}{z_2}, z_3, z_4, -\mathbf{t}_3, -\mathbf{t}_4 \right), \tag{21}$$

which acts on cameras as

$$H_2 = \mathrm{diag}(-1, -1, -1, 1) \sim \mathrm{diag}(1, 1, 1, -1) \in \mathrm{S}(3). \tag{22}$$

For $j = 3$,

$$\Psi_3(x_2, x_3, x_4, y_2, y_3, y_4, z_2, z_3, z_4, \mathbf{t}_3, \mathbf{t}_4)$$
$$= \left(x_2, \frac{y_3}{z_3}, x_4, y_2, \frac{-x_3}{z_3}, y_4, z_2, \frac{-1}{z_3}, z_4, -\mathbf{t}_3, \mathbf{t}_4 \right), \tag{23}$$

and for $j = 4$,

$$\Psi_4(x_2, x_3, x_4, y_2, y_3, y_4, z_2, z_3, z_4, \mathbf{t}_3, \mathbf{t}_4)$$
$$= \left(x_3, x_4, \frac{y_4}{z_4}, y_2, y_3, \frac{-x_4}{z_4}, z_2, z_3, \frac{-1}{z_4}, \mathbf{t}_3, -\mathbf{t}_4 \right), \tag{24}$$

both of which act on cameras as

$$H_3 = H_4 = \mathrm{diag}(-1, -1, -1, -1) \sim I \in \mathrm{S}(3). \tag{25}$$

We summarize the important properties of the symmetry group generated by $\Psi_1, \ldots, \Psi_4$ in the next proposition.

Proposition 4. Each symmetry Ψ_j for $j = 1, 2, 3, 4$ defined in Eqs. (19), (21), (23) and (24) preserves solutions to the 13 point problem in Cayley parameters, and induces a camera transformation $(P_1, \ldots, P_4) \mapsto (P_1 H_j, \ldots, P_4 H_j)$. Moreover, one solution in calibrated camera matrices is chiral (cf. [35, Prop. 10]) iff its entire orbit of 16 solutions under the group generated by $\Psi_1, \ldots, \Psi_4$ is.

Proof. All claims but the last may be verified by direct calculation. For the last, note that for generic $(P_1, \ldots, P_4)$ we can uniquely recover a scene point $\mathbf{X}_j \in \mathbb{P}^3$ from its images $\mathbf{l}_{1j}, \ldots, \mathbf{l}_{4j} \in \mathbb{P}^1$. We assume the last coordinate of $\mathbf{X}_j$ equals 1. To enforce that $\mathbf{X}_j$ lies in front of any associated pinhole camera, we recall the chirality constraint used in [63, § 2.2]. Let $\mathbf{x}_{ij} \in \mathbb{R}^2$ be an image point in pixel coordinates corresponding to $\mathbf{l}_{ij}$. Eq. (1) implies that $P_i \mathbf{X}_j$ is the direction vector of the radial line through the projected point. For $\mathbf{X}_j$ to lie in front of an associated pinhole camera, we must have

$$\mathbf{x}_{ij}^T P_i \mathbf{X}_j > 0 \quad \forall i. \tag{26}$$

Now, fixing $i_1, \ldots, i_4 \in \{0, 1\}$, we may consider the transformed arrangement $(\tilde{P}_1, \ldots, \tilde{P}_4)$ defined by setting $\tilde{P}_i := P_i H$, where $H = H_1^{i_1} H_2^{i_2} H_3^{i_3} H_4^{i_4}$. Then, for the transformed world point $\tilde{\mathbf{X}}_j = H^{-1} \mathbf{X}_j$, Eq. (26) and the fact that $\mathbf{x}_{ij}^T P_i \mathbf{X}_j = \mathbf{x}_{ij}^T \tilde{P}_i \tilde{\mathbf{X}}_j$ gives the last claim. $\qquad\square$

Next, we verify that the metric upgrade of Proposition 1 works as expected.

Proposition 5. If H in (13) has full rank, then all four transformed radial cameras $P_1 H, \ldots, P_4 H$ are calibrated.

Proof. Let $\Omega = \mathrm{diag}(1, 1, 1, 0)$ be the symmetric matrix that represents the *dual absolute quadric*. Then, a radial camera P_k is calibrated if and only if

$$(P_k \Omega)(P_k \Omega)^T = P_k \Omega P_k^T \sim I_{2 \times 2}. \tag{27}$$

Letting $\tilde{P}_i = P_i H$ be the transformed camera for each $i = 1, \ldots 4$, we calculate

$$\begin{aligned}
(\tilde{P}_i \Omega)(\tilde{P}_i \Omega)^T &= (P_i H \Omega)(P_i H \Omega)^T \\
&\sim P_i H \Omega^2 H^T P_i^T \\
&\sim P_i V \, \mathrm{diag}(\lambda_1^2, \lambda_2^2, \lambda_3^2, 0) V^T P_i^T \\
&\sim P_i Q P_i^T \\
&\sim I_{2 \times 2}. \qquad\square
\end{aligned}$$

# solutions	group	group order
13-pt		
28	$\bar{S}_{28}$	$28!$
56	$S_2 \wr S_{28} \cap A_{56} \cong (S_2^{28} \cap A_{56}) \rtimes G_{28}$	$28! \cdot 2^{27}$
224	$((S_2 \times S_2) \rtimes S_4)^{28} \rtimes G_{56}$	$28! \cdot 2^{27} \cdot (4 \cdot 4!)^{28}$
3584	$S_2^{364} \rtimes G_{224}$	$28! \cdot 2^{27} \cdot (4 \cdot 4!)^{28} \cdot 2^{364}$
7-pt		
25	$\bar{S}_{25}$	$25!$
50	$S_2 \wr S_{25} \cong S_2^{25} \rtimes G_{25}$	$25! \cdot 2^{25}$

Table 3. We computed Galois/monodromy permutations for each each of the different problem formulations For readability, G_n denotes the Galois group associated to a problem formulation with n complex solutions.

7.3. Internal constraints

This section presents details for the construction of internal constraints of radial quadrifocal tensors. We prove the result for the vanishing ideal of upright quadrifocal tensor and link historical Nanson's equations, which define the internal constraints for a general quadrifocal tensor, to their modern treatment using cycle-sums.

For the upright case, we now describe the *vanishing ideal* [16, Def. 5, p. 32] of the image of the map

$$\Psi_{\mathrm{up}} : \mathbb{R}^7 \dashrightarrow \mathbb{P}^{15},$$
$$(y_2, y_3, t_{31}, t_{32}, y_4, t_{41}, t_{42}) \mapsto T_{P_1(\mathbf{y},\mathbf{t}),\dots,P_4(\mathbf{y},\mathbf{t})}.$$

from Section 4.2. The next result is that this ideal is generated by the eight equations we discovered via elimination. The polynomials $f_{\mathrm{up}}(T)$ and $g_{\mathrm{up}}(T)$ have degree 5 and 22 and 52 terms, respectively. We do not know of any compact formula for them. For completeness, we supply the following Macaulay2 [30] code that can be used to compute them.

```
FF = QQ;
R = FF[c2,s2,c3,s3,t31,t32,c4,s4,t41
    ,t42]/ideal(s2^2+c2^2-1,s3^2+c3
    ^2-1,s4^2+c4^2-1);
I4 = id_(R^4);
P1 = matrix {{1_FF, 0, 0, 0}, {0, 1
    _FF, 0, 0}};
P2 = matrix {{c2, 0, s2, 0}, {0, 1,
    0, 1}};
P3 = matrix {{c3, 0, s3, t31}, {0,
    1, 0, t32}};
P4 = matrix {{c4, 0, s4, t41}, {0,
    1, 0, t42}};
stackedCameras = P1||P2||P3||P4;
quad = toList apply((0,0,0,0)
    ..(1,1,1,1), (i,j,k,l) -> (-1)^(
    i+j+k+l)* det stackedCameras^{i
    ,2+j,4+k,6+l}_{0,1,2,3});
S = FF[T_(0,0,0,0)..T_(1,1,1,1)];
phi = map(R,S,quad);
J = ker(phi, SubringLimit=>9);
```

```
nonlinearConstraints = select(J_*, p
    -> (first degree p) > 2);
(fup, gup) = (first
    nonlinearConstraints, last
    nonlinearConstraints)
```

Proposition 6. The vanishing ideal of all upright radial quadrifocal tensors (that is, the image of Ψ_{up}) is generated by two degree-5 homogeneous forms $f_{\mathrm{up}}(T)$, $g_{\mathrm{up}}(T)$ and the variables $T_{0,0,0,0}, T_{1,1,1,1}, T_{1,1,1,0}, T_{1,1,0,1}, T_{1,0,1,1}, T_{0,1,1,1,1}$.

The above Macaulay2 computation, if run without the option SubringLimit, would return a complete set of generators of the vanishing ideal. However, this did not terminate after a day of computation. Instead, we can argue using basic commutative algebra, similar to an argument given in [61, Thm. 1.1].

Proof. Let $X \subset \mathbb{P}_{\mathbb{C}}^{15}$ be the the complexified image of Ψ_{up}, and $Y = \mathrm{V}(J) \subset \mathbb{P}_{\mathbb{C}}^{16}$ be the projective vanishing locus of the eight polynomials which generate the ideal J. Then $X \subset Y$, and X has a unirational parametrization, whose Jacobian we can evaluate at a rational point to deduce that $\dim(X) \geq 7$. On the other hand, computing a partial Gröbner basis of the ideal J allows us to check that $\dim(Y) \leq 7$, from which we may conclude that $\dim(X) = \dim(Y) = 7$ and that X is an irreducible component of Y. Since the ideal J generated by the 8 polynomials is a complete intersection, it follows from Macaulay's unmixedness theorem [22, Thm. 18.14] that Y is equidimensional and J has no embedded primes. To prove J is prime, it is enough to show that Y is irreducible and that J is radical. Irreducibility of Y can be proved by checking that $\deg(X) = \deg(Y) = 25 = \deg f_{\mathrm{up}} \cdot \deg g_{\mathrm{up}}$. Indeed,

$$25 \leq \deg(X)$$
$$\leq \deg(Y)$$
$$\leq 25.$$

4

The last inequality above holds by Bézout's theorem. The first can be checked by producing a single problem instance with at least 25 complex solutions in tensors. More precisely, we fabricate random rational data in $\mathbf{l}_{ij} \in \mathbb{P}^1$ and check that the equations (2) give us radical zero-dimensional ideals in cameras and tensors of the respective expected degrees 50 and 25. These computations also show J is generically-reduced, from which it follows, since J is Cohen-Macaulay, that J is radical. We may conclude that J is the prime vanishing ideal of X. $\qquad\square$

Next, we define Nanson's equations discussed in Section 4.1, which give a subset of the internal constraints in the general case. We recall from Sec. 4 that internal constraints on quadrifocal tensors are the same as homogeneous polynomials vanishing on the image of the *projective principal minor map*,

$$\Phi : \mathbb{R}^{4\times 4} \dashrightarrow \mathbb{P}^{15},$$
$$X \mapsto \left[A_S(X) \mid S \subset \{1,2,3,4\}\right].$$

As noted in the introduction, the first set of equations vanishing on the image of Φ was produced by Nanson [55]. Lin and Sturmfels [48] gave an interpretation of Nanson's relations in terms of *cycle sums*. They also observed that Nanson's equations were not sufficient to generate the prime ideal of all polynomials vanishing on the image of Φ, and they produced 718 linearly independent polynomials of degree 12 which they proved determine the radial quadrifocal variety as a subscheme of $\mathbb{P}^{15}$. Work of Borodin and Rains [7] also stated the existence of these 718 polynomials, and the fact that a projective variety of dimension 13 and degree 28.

Following [48, Prop. 3], we may define 15 cycle-sum polynomials $C_I(X)$ in the entries of a 4×4 matrix X as follows. For each nonempty $I \subset \{1,2,3,4\}$ of size d, define

$$C_I(X) = \sum_{I = I_1 \sqcup \cdots I_k} (-1)^{k+d}(k-1)!\, A_{I_1}(X) \cdots A_{I_k}(X),$$
$$(28)$$

where the sum is taken over all partitions of the set I. Nanson's matrix $\mathbf{N} = \begin{bmatrix} \mathbf{n}_1 & | & \mathbf{n}_2 & | & \mathbf{n}_3 & | & \mathbf{n}_4 \end{bmatrix}$ can be expressed

in terms of the cycle-sums (cf. Eq. (28)) as follows:

$$\mathbf{n}_1 = \begin{bmatrix} C_{1,2,3}(X)C_{1,4}(X) \\ C_{1,2,4}(X)C_{2,3}(X) \\ C_{1,3,4}(X)C_{2,3}(X) \\ C_{2,3,4}(X)C_{1,4}(X) \\ 1 \end{bmatrix},$$

$$\mathbf{n}_2 = \begin{bmatrix} C_{1,2,4}(X)C_{1,3}(X) \\ C_{1,2,4}(X)C_{2,3}(X) \\ C_{1,3,4}(X)C_{2,3}(X) \\ C_{2,3,4}(X)C_{1,3}(X) \\ 1 \end{bmatrix},$$

$$\mathbf{n}_3 = \begin{bmatrix} C_{1,3,4}(X)C_{1,2}(X) \\ C_{2,3,4}(X)C_{1,2}(X) \\ C_{1,2,3}(X)C_{3,4}(X) \\ C_{1,2,4}(X)C_{3,4}(X) \\ 1 \end{bmatrix},$$

$$\mathbf{n}_4 = \begin{bmatrix} 2C_{2,3,4}(X)C_{1,2}(X)C_{1,3}(X)C_{1,4}(X) + C_{1,3,4}(X)C_{1,2,4}(X)C_{1,2,3}(X) \\ 2C_{1,3,4}(X)C_{1,2}(X)C_{2,3}(X)C_{2,4}(X) + C_{2,3,4}(X)C_{1,2,4}(X)C_{1,2,3}(X) \\ 2C_{1,2,4}(X)C_{1,3}(X)C_{2,3}(X)C_{3,4}(X) + C_{2,3,4}(X)C_{1,3,4}(X)C_{1,2,3}(X) \\ 2C_{1,2,3}(X)C_{1,4}(X)C_{2,4}(X)C_{3,4}(X) + C_{2,3,4}(X)C_{1,3,4}(X)C_{1,2,4}(X) \\ C_{1,2,3,4}(X) \end{bmatrix}.$$
$$(29)$$

Finally, we provide an alternative formula for the Hartley-Schaffalitzky map defined in Equation (6).

$$\begin{bmatrix} \psi_{\mathrm{HS}}(P_1) \\ \psi_{\mathrm{HS}}(P_2) \\ \psi_{\mathrm{HS}}(P_3) \\ \psi_{\mathrm{HS}}(P_4) \end{bmatrix} = D_{8\times 8}(p) \cdot T(p) \cdot D_{4\times 4}(p), \quad \text{where}$$

$$D_{8\times 8}(p) = \mathrm{diag}\left(1, 1, \frac{p_{21}}{p_{11}}, \frac{p_{21}}{p_{11}}, \frac{p_{31}}{p_{11}}, \frac{p_{31}}{p_{11}}, \frac{p_{41}}{p_{11}}, \frac{p_{41}}{p_{11}}\right),$$

$$D_{4\times 4}(p) = \mathrm{diag}\left(1, \frac{p_{11}}{p_{21}}, \frac{p_{11}}{p_{31}}, \frac{p_{11}}{p_{41}}\right),$$

$$T(p) = \begin{bmatrix} 1 & 0 & 0 & 0 \\ p_{11} & p_{21} & p_{31} & p_{41} \\ 0 & 1 & 0 & 0 \\ p_{11} & p_{22} & p_{32} & p_{42} \\ 0 & 0 & 1 & 0 \\ p_{11} & p_{23} & p_{33} & p_{43} \\ 0 & 0 & 0 & 1 \\ p_{11} & p_{24} & p_{34} & p_{44} \end{bmatrix}.$$
$$(30)$$

Note that $T(p)$ is formed by transposing the interleaved non-identity 4×4 matrix formed by each camera's second row (cf. [32, § 2.2]).

The group $\mathbb{Z}_2 \rtimes (S_4 \rtimes \mathrm{GL}_2^4)$ acts on 8×4 matrices $[A, B]^\top$ and preserves the set of special maximal minors of $[A, B]^\top$, or the principal minors of $A^{-1}B$ [39]. Let $\mathbb{Z}_2 \rtimes \mathbb{T}^4$ denote the subgroup where the $\mathbb{Z}_2$ is the transpose action and $\mathbb{T}^4$ is the 4-dimensional torus of non-zero scalars acting by conjugation. It is straightforward to check that $\mathbb{Z}_2 \rtimes \mathbb{T}^4$ does not change the values of the principal minors, and moreover, we have presented the HS symmetry as an element of this group.

8. Cameras from Radial Quadrifocal Tensors

Here, we describe details of a method used for recovering uncalibrated cameras in the form (5) from a radial

quadrifocal tensor estimated using either the linear method or the "Implicit 13" solver. This method does not assume any constraints on a radial quadrifocal tensor. It sends "slightly incorrect" radial quadrifocal tensors to "slightly incorrect" camera matrices.

Having recovered a quadrifocal tensor $T \in \mathbb{R}^{2\times2\times2\times2}$, we may, assuming genericity, rescale it so that $T_{0,0,0,0} = 1$. With respect to our standard form, several camera parameters are rational functions in T:

$$
\begin{aligned}
p_{44} &= -T_{0,0,0,1} \\
p_{33} &= -T_{0,0,1,0} \\
p_{22} &= -T_{0,1,0,0} \\
p_{11} &= -T_{1,0,0,0} \\
p_{41} &= p_{44} - \frac{T_{1,0,0,1}}{p_{11}} \\
p_{31} &= p_{33} - \frac{T_{1,0,1,0}}{p_{11}} \\
p_{21} &= p_{22} - \frac{T_{1,1,0,0}}{p_{11}}.
\end{aligned}
\tag{31}
$$

In principle, solving a single quadratic equation is sufficient to recover the remaining 6 unknowns $p_{23}, p_{32}, p_{24}, p_{42}, p_{34}, p_{43}$, but this assumes that the tensor entries are known to exactly satisfy all internal constraints on radial quadrifocal tensors. This assumption almost surely fails for the linear method, and the same is true for the minimal solver due to the inherent inexactness of polynomial system solving. Nevertheless, when using either method we may recover 8 candidates for the remaining unknowns by solving three independent quadratic equations. We describe a method for recovering candidates for the pair (p_{23}, p_{32}): the other pairs (p_{24}, p_{42}), (p_{34}, p_{43}) may be treated similarly.

To recover the pair (p_{23}, p_{32}), we use the equations

$$
\begin{aligned}
T_{0,1,1,0} &= \underline{p_{23}}\,\underline{p_{32}} - p_{22}p_{33} \\
T_{1,0,0,0} &= p_{11}p_{22}p_{31} - p_{11}\underline{p_{23}}p_{31} - p_{11}p_{21}\underline{p_{32}} + \dots \\
&\quad p_{11}\underline{p_{23}}\,\underline{p_{32}} + p_{11}p_{21}p_{33} - p_{11}p_{22}p_{33},
\end{aligned}
\tag{32}
$$

where, using (31), we have underlined the only unknown quantities. Thus, subtracting p_{11} times the first equation from the second, we obtain an affine-linear equation in the unknown pair, which lets us write

$$
p_{32} = \frac{a}{b + cp_{23}}
\tag{33}
$$

for some scalars $a, b, c \in \mathbb{R}$. Substituting (33) into either of the equations in (32) and clearing denominators, we obtain a single quadratic equation in the unknown p_{23}.

After solving all 3 pairs of quadratic equations, we get 8 possible decompositions of the quadrifocal tensor T.

If tensor T does not exactly fulfill the internal constraints, this previously-described procedure is not optimal, since the elements $T_{0,1,1,1}$ and $T_{1,1,1,1}$ are not considered in the recovery procedure described above. This often happens for both the 15 point linear solver, and the 13 point implicit solver, as the 15 point linear solver does not consider any internal constraints, while the 13 point implicit solver is somewhat unstable. Therefore, we propose a local optimization step, which starts from cameras P_1, P_2, P_3, P_4, and performs 3 steps of the Gauss-Newton method to minimize the sum of squared differences between each of the 16 elements of the tensor T, and the corresponding elements calculated from the unknowns by equation (3) from the main paper. We have observed that the local optimization improves the rotation and translation error, on average by 2-3 decimal positions.

9. Additional experiments

Here, we give an additional experimental evalution of the proposed method. For the evaluation, we consider two datasets *Grossmunster* and *Kirchenge* from Larsson et al. [47], and 11 scenes from ETH3D [71]. For each dataset, we randomly sample 200 sets of 4 images which share at least 50 3D points in the ground truth reconstruction. Table 4 presents a more detailed evaluation of the experiment shown in Table 2 in the main paper. For every considered solver (Linear, 13 Explicit, 13 Implicit, 7 Explicit, 7 Implicit), we give the fraction of the scenes whose rotation and translation error are below given thresholds. Namely, we consider thresholds $5°$, $10°$, $20°$ for rotation, and $10cm$, $20cm$, and $50cm$ for translation. The table shows that both "13 Explicit" and "13 Implicit" are consistently more successful than the "Linear" solver. The 7 point upright solvers reach good results for datasets whose cameras satisfy the upright constraint.

In Figures 7–9 we show more qualitative results from integrating the radial quadrifocal solver into the 1D radial Structure-from-Motion pipeline from Larsson et al. [47].

Figure 7. Qualitative results of 1D radial Structure-from-Motion on the *Eglise* dataset (85 images) from [62].
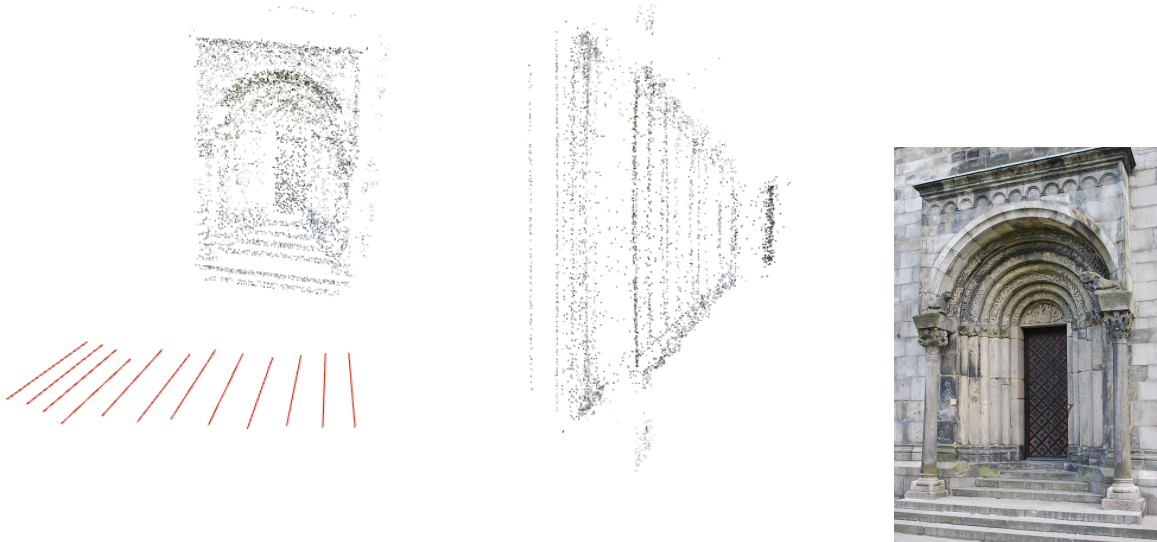

Figure 8. Qualitative results of 1D radial Structure-from-Motion on the *Door* dataset (12 images) from [62].
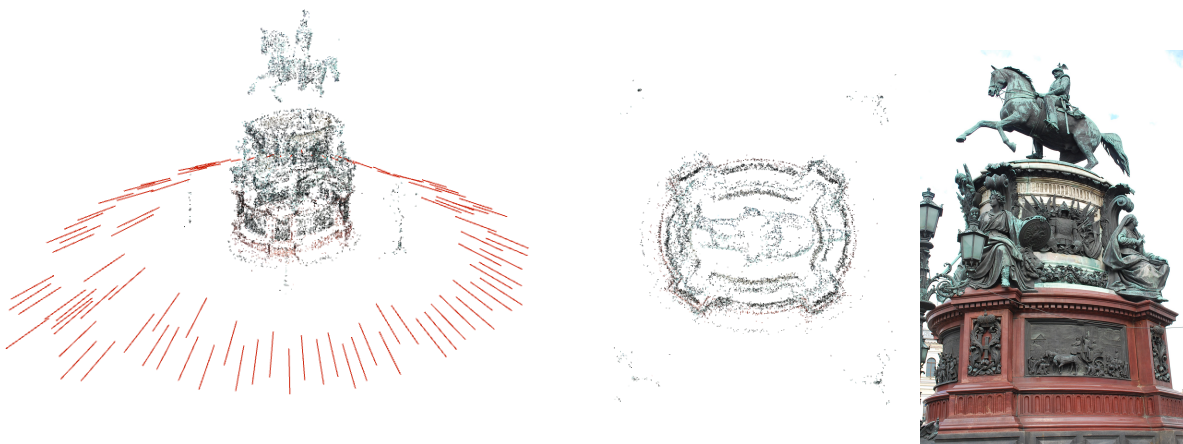

Figure 9. Qualitative results of 1D radial Structure-from-Motion on the *Nikolai* dataset (89 images) from [62].

7

Dataset, # tuples	Solver	Rotation error			Translation		
		$< 5°$	$< 10°$	$< 20°$	$< 10cm$	$< 20cm$	$< 50cm$
Grossmunster	Linear	0.25	0.33	0.42	0.15	0.36	0.8
	13 Explicit	**0.28**	**0.35**	**0.51**	**0.28**	**0.53**	**0.82**
	13 Implicit	0.26	0.33	0.46	0.22	0.47	0.81
200 tuples	7 Explicit	0.02	0.06	0.15	0.11	0.32	0.78
	7 Implicit	0.02	0.04	0.12	0.08	0.26	0.75
Kirchenge	Linear	0.27	0.31	0.43	0.21	0.41	0.83
	13 Explicit	**0.32**	**0.41**	**0.54**	0.21	**0.45**	**0.89**
	13 Implicit	0.31	0.39	0.50	**0.23**	0.44	0.86
200 tuples	7 Explicit	0.01	0.03	0.09	0.09	0.23	0.79
	7 Implicit	0.01	0.01	0.10	0.05	0.24	0.77
Courtyard	Linear	**0.04**	**0.11**	**0.28**	0.09	0.24	0.65
	13 Explicit	0.03	**0.11**	0.26	0.02	0.11	0.51
	13 Implicit	0.02	0.08	0.25	0.04	0.18	0.65
200 tuples	7 Explicit	0.03	0.09	0.19	**0.13**	**0.31**	0.67
	7 Implicit	0.03	0.10	0.22	0.08	0.29	**0.68**
Delivery	Linear	0.15	0.24	0.44	0.28	0.51	0.89
	13 Explicit	0.14	0.22	0.43	0.23	0.43	0.8
	13 Implicit	**0.17**	**0.26**	0.44	**0.34**	**0.59**	**0.94**
200 tuples	7 Explicit	0.09	0.23	**0.46**	0.32	0.58	0.91
	7 Implicit	0.05	0.13	0.34	0.33	0.54	0.90
Electro	Linear	0.12	0.19	0.40	0.33	0.64	0.92
	13 Explicit	0.12	0.2	0.38	0.32	0.53	0.89
	13 Implicit	0.06	0.17	0.34	0.29	0.61	0.90
200 tuples	7 Explicit	**0.16**	**0.27**	**0.44**	**0.47**	**0.72**	**0.94**
	7 Implicit	0.07	0.14	0.29	0.41	0.63	0.9
Facade	Linear	0.26	0.41	0.61	0.06	0.13	0.41
	13 Explicit	**0.33**	**0.52**	**0.68**	0.05	0.12	0.36
	13 Implicit	0.23	0.42	0.56	0.07	0.16	**0.47**
200 tuples	7 Explicit	0.14	0.28	0.44	**0.08**	**0.19**	0.45
	7 Implicit	0.11	0.24	0.45	0.05	0.14	0.41
Office	Linear	0.02	0.17	0.28	0.91	1.0	1.0
	13 Explicit	**0.17**	**0.30**	0.41	0.78	1.0	1.0
	13 Implicit	0.15	0.28	**0.44**	0.94	1.0	1.0
168 tuples	7 Explicit	0.0	0.0	0.0	**1.0**	1.0	1.0
	7 Implicit	0.02	0.07	0.20	0.94	1.0	1.0
Pipes	Linear	0.31	0.38	0.44	**1.0**	1.0	1.0
	13 Explicit	**0.44**	**0.5**	0.57	0.88	1.0	1.0
	13 Implicit	0.38	**0.5**	**0.75**	**1.0**	1.0	1.0
28 tuples	7 Explicit	0.38	0.38	0.5	0.94	1.0	1.0
	7 Implicit	0.13	0.13	0.19	**1.0**	1.0	1.0
Playground	Linear	0.18	0.23	0.37	0.46	0.76	0.98
	13 Explicit	**0.2**	**0.27**	**0.39**	0.33	0.62	0.95
	13 Implicit	0.19	0.26	0.37	**0.48**	**0.79**	**0.99**
200 tuples	7 Explicit	0.04	0.04	0.08	0.31	0.75	0.97
	7 Implicit	0.01	0.04	0.08	0.31	0.71	**0.99**
Relief	Linear	0.21	0.29	0.43	0.38	0.59	0.91
	13 Explicit	**0.22**	0.34	**0.52**	0.34	0.61	0.96
	13 Implicit	**0.22**	**0.38**	**0.52**	**0.45**	**0.62**	0.98
200 tuples	7 Explicit	0.01	0.02	0.04	0.32	0.6	0.98
	7 Implicit	0.01	0.01	0.07	0.27	0.61	**0.99**
Relief 2	Linear	**0.40**	**0.44**	**0.55**	0.39	0.6	0.7
	13 Explicit	0.26	0.40	**0.55**	0.48	0.79	**1.0**
	13 Implicit	0.22	0.37	0.53	**0.6**	**0.89**	**1.0**
200 tuples	7 Explicit	0.05	0.07	0.12	0.45	0.91	**1.0**
	7 Implicit	0.03	0.06	0.09	0.43	0.90	**1.0**
Terrace	Linear	0.09	0.17	0.33	0.31	0.60	0.90
	13 Explicit	**0.10**	**0.19**	**0.40**	0.26	0.48	0.86
	13 Implicit	0.08	0.13	0.27	0.33	0.62	0.90
200 tuples	7 Explicit	0.05	0.13	0.28	**0.46**	**0.82**	**0.98**
	7 Implicit	0.05	0.11	0.27	0.38	0.65	0.92
Terrains	Linear	0.19	0.3	0.49	0.62	0.81	0.93
	13 Explicit	0.2	0.35	0.51	0.48	0.79	0.98
	13 Implicit	0.11	0.25	0.42	0.65	0.91	**0.99**
200 tuples	7 Explicit	**0.31**	**0.49**	**0.65**	**0.78**	**0.93**	**0.99**
	7 Implicit	0.2	0.4	0.60	**0.78**	**0.93**	0.98

Table 4. **Real tests on datasets** [47], [71]. Detailed evaluation of the experiment in Table 2. We report the fraction of poses whose rotation and translation errors are below given thresholds.

References

[1] S. Agarwal, N. Snavely, I. Simon, S. M. Seitz, and R. Szeliski, *Building Rome in a day*, IEEE 12th International Conference on Computer Vision, ICCV 2009, Kyoto, Japan, September 27 - October 4, 2009, 2009, pp. 72–79. ↑1

[2] A. A. Ahmadieh and C. Vinzant, *Determinantal representations and the image of the principal minor map*, arXiv 2205.05267, 2022. ↑5

[3] E. Ask, Y. Kuang, and K. Åström, *Exploiting p-fold symmetries for faster polynomial equation solving*, Proceedings of the 21st International Conference on Pattern Recognition, ICPR 2012, Tsukuba, Japan, November 11-15, 2012, 2012, pp. 3232–3235. ↑3

[4] C. Bajaj, *The algebraic degree of geometric optimization problems*, Discrete & Computational Geometry **3** (1988), no. 2, 177–191. ↑3

[5] D. Barath, T. Toth, and L. Hajder, *A minimal solution for two-view focal-length estimation using two affine correspondences*, 2017 IEEE Conference on Computer Vision and Pattern Recognition, CVPR 2017, Honolulu, HI, USA, July 21-26, 2017, 2017, pp. 2557–2565. ↑2

[6] S. Bhayani, Z. Kukelova, and J. Heikkilä, *A Sparse Resultant Based Method for Efficient Minimal Solvers*, 2020 IEEE/CVF conference on computer vision and pattern recognition, CVPR 2020, Seattle, WA, USA, June 13-19, 2020, 2020, pp. 1767–1776. ↑2, 3

[7] A. Borodin and E. M. Rains, *Eynard-Mehta theorem, Schur process, and their Pfaffian analogs*, Journal of Statistical Physics **121** (2005), no. 3-4, 291–317. MR2185331 ↑5

[8] P. Breiding, F. Rydell, E. Shehu, and A. Torres, *Line multiview varieties* (2022). ↑3

[9] P. Breiding and S. Timme, *Homotopycontinuation.jl: A package for homotopy continuation in julia*, Mathematical software – icms 2018, 2018, pp. 458–465. ↑2

[10] T. Brysiewicz, J. I. Rodriguez, F. Sottile, and T. Yahl, *Solving decomposable sparse systems*, Numerical Algorithms (2021). ↑5

[11] M. Byröd, K. Josephson, and K. Åström, *A Column-Pivoting Based Strategy for Monomial Ordering in Numerical Gröbner Basis Calculations*, Computer Vision - ECCV 2008, Marseille, France, October 12-18, 2008, Proceedings, Part IV, 2008, pp. 130–143. ↑2

[12] F. Camposeco, T. Sattler, and M. Pollefeys, *Minimal Solvers for Generalized Pose and Scale Estimation from Two Rays and One Point*, ECCV – European Conference on Computer Vision, 2016, pp. 202–218. ↑2

[13] M. K. Chandraker, S. Agarwal, F. Kahl, D. Nistér, and D. J. Kriegman, *Autocalibration via rank-constrained estimation of the absolute quadric*, 2007 IEEE Computer Society Conference on Computer Vision and Pattern Recognition (CVPR 2007), 18-23 June 2007, Minneapolis, Minnesota, USA, 2007. ↑4

[14] C. Chien, H. Fan, A. Abdelfattah, E. P. Tsigaridas, S. Tomov, and B. B. Kimia, *GPU-based homotopy continuation for minimal problems in computer vision*, IEEE/CVF Conference on Computer Vision and Pattern Recognition, CVPR 2022, New Orleans, LA, USA, June 18-24, 2022, 2022, pp. 15744–15755. ↑3

[15] O. Chum, J. Matas, and J. Kittler, *Locally optimized RANSAC*, Joint Pattern Recognition Symposium, 2003, pp. 236–243. ↑7

[16] D. A. Cox, J. Little, and D. O'Shea, *Ideals, varieties, and algorithms*, 4ed., Undergraduate Texts in Mathematics, Springer, 2015. MR3330490 ↑5, 4

[17] F. Dellaert and A. W. Stroupe, *Linear 2D Localization and Mapping for Single and Multiple Robot Scenarios*, Proceedings of the 2002 IEEE International Conference on Robotics and Automation, ICRA 2002, May 11-15, 2002, Washington, DC, USA, 2002, pp. 688–694. ↑2

[18] T. Duff, C. Hill, A. Jensen, K. Lee, A. Leykin, and J. Sommars, *Solving polynomial systems via homotopy continuation and monodromy*, IMA Journal of Numerical Analysis (2018). ↑4, 6

[19] T. Duff, K. Kohn, A. Leykin, and T. Pajdla, *PLMP - Point-line Minimal Problems in Complete Multi-view Visibility*, 2019 IEEE/CVF International Conference on Computer Vision, ICCV 2019, Seoul, Korea (South), October 27 - November 2, 2019, 2019, pp. 1675–1684. ↑3

[20] _____, *PL₁P - point-line minimal problems under partial visibility in three views*, Computer Vision - ECCV 2020 - 16th European Conference, Glasgow, UK, August 23-28, 2020, Proceedings, Part XXVI, 2020, pp. 175–192. ↑3

[21] T. Duff, V. Korotynskiy, T. Pajdla, and M. H. Regan, *Galois/monodromy groups for decomposing minimal problems in 3D reconstruction*, To appear in SIAM Journal on Applied Algebra and Geometry (2022), available at `arXiv2105.04460`. ↑3, 2

[22] D. Eisenbud, *Commutative Algebra*, Graduate Texts in Mathematics, vol. 150, Springer-Verlag, New York, 1995. With a view toward algebraic geometry. ↑4

[23] A. Elqursh and A. M. Elgammal, *Line-based relative pose estimation*, The 24th IEEE Conference on Computer Vision and Pattern Recognition, CVPR 2011, Colorado Springs, CO, USA, 20-25 June 2011, 2011, pp. 3049–3056. ↑2

[24] R. Fabbri, T. Duff, H. Fan, M. H. Regan, D. da Costa de Pinho, E. P. Tsigaridas, C. W. Wampler, J. D. Hauenstein, P. J. Giblin, B. B. Kimia, A. Leykin, and T. Pajdla, *TRPLP - Trifocal Relative Pose From Lines at Points*, 2020 IEEE/CVF Conference on Computer Vision and Pattern Recognition, CVPR 2020, Seattle, WA, USA, June 13-19, 2020, 2020, pp. 12070–12080. ↑2, 3, 6

[25] H. Fan, J. Kileel, and B. B. Kimia, *On the Instability of Relative Pose Estimation and RANSAC's Role*, IEEE/CVF Conference on Computer Vision and Pattern Recognition, CVPR 2022, New Orleans, LA, USA, June 18-24, 2022, 2022, pp. 8925–8933. ↑3

[26] O. D. Faugeras, Q. Luong, and S. J. Maybank, *Camera Self-Calibration: Theory and Experiments*, Computer Vision - ECCV'92, Second European Conference on Computer Vision, Santa Margherita Ligure, Italy, May 19-22, 1992, Proceedings, 1992, pp. 321–334. ↑2

[27] O. D. Faugeras, L. Quan, and P. F. Sturm, *Self-Calibration of a 1D Projective Camera and its Application to the self-calibration of a 2D projective camera*, IEEE Transactions on Pattern Analysis and Machine Intelligence **22** (2000), no. 10, 1179–1185. ↑2

[28] M. A. Fischler and R. C. Bolles, *Random sample consensus: a paradigm for model fitting with applications to image analysis and automated cartography*, Communications of the ACM **24** (1981), no. 6, 381–395. ↑3

[29] F. Fraundorfer, P. Tanskanen, and M. Pollefeys, *A Minimal Case Solution to the Calibrated Relative Pose Problem for the Case of Two Known Orientation Angles*, Computer Vision - ECCV 2010, 11th European Conference on Computer Vision, Heraklion, Crete, Greece, September 5-11, 2010, Proceedings, Part IV, 2010, pp. 269–282. ↑2

[30] D. R. Grayson and M. E. Stillman, *Macaulay2, a software system for research in algebraic geometry*. Available at `http://www.math.uiuc.edu/Macaulay2/`. ↑2, 4

[31] R. Hartley and F. Schaffalitzky, *Reconstruction from projections using Grassmann tensors*, Computer Vision - ECCV 2004, 2004, pp. 363–375. ↑2

[32] _____, *Reconstruction from projections using Grassmann tensors*, International Journal of Computer Vision **83** (2009), no. 3, 274–293 (English). ↑2, 4, 5

[33] R. Hartley and A. Zisserman, *Multiple view geometry in Computer Vision*, Second, Cambridge University Press, Cambridge, 2003. With a foreword by Olivier Faugeras. ↑1, 2, 4

[34] R. I. Hartley, *In Defence of the 8-Point Algorithm*, Procedings of the Fifth International Conference on Computer Vision (ICCV 95), Massachusetts Institute of Technology, Cambridge, Massachusetts, USA, June 20-23, 1995, 1995, pp. 1064–1070. ↑2

[35] ――――, *Chirality*, International Journal of Computer Vision **26** (1998), no. 1, 41–61. ↑6, 3

[36] J. D. Hauenstein and M. H. Regan, *Adaptive strategies for solving parameterized systems using homotopy continuation*, Applied Mathematics and Computation **332** (2018), 19–34. MR3788668 ↑3

[37] J. D. Hauenstein, J. I. Rodriguez, and F. Sottile, *Numerical computation of galois groups*, Foundations of Computational Mathematics **18** (2018), no. 4, 867–890. ↑3

[38] O. Hesse, *Die cubische Gleichung, von welcher die Lösung des Problems der Homographie von M. Chasles abhängt*, Journal für die Reine und Angewandte Mathematik **62** (1863), 188–192. MR1579236 ↑2

[39] O. Holtz and B. Sturmfels, *Hyperdeterminantal relations among symmetric principal minors*, Journal of Algebra **316** (2007), no. 2, 634–648. ↑2, 5, 3

[40] P. Hruby, T. Duff, A. Leykin, and T. Pajdla, *Learning to solve hard minimal problems*, IEEE/CVF Conference on Computer Vision and Pattern Recognition, CVPR 2022, New Orleans, LA, USA, June 18-24, 2022, 2022, pp. 5522–5532. ↑2, 3, 5

[41] H. Huang and L. Oeding, *Symmetrization of principal minors and cycle-sums*, Linear Multilinear Algebra **65** (2017), no. 6, 1194–1219. MR3615538 ↑5

[42] J. Kileel, *Minimal problems for the calibrated trifocal variety*, SIAM Journal on Applied Algebra and Geometry **1** (2017), no. 1, 575–598. MR3705779 ↑3

[43] L. Kneip, R. Siegwart, and M. Pollefeys, *Finding the exact rotation between two images independently of the translation*, ECCV – European Conference on Computer Vision, 2012, pp. 696–709. ↑2

[44] Z. Kukelova, M. Bujnak, and T. Pajdla, *Automatic generator of minimal problem solvers*, ECCV – European Conference on Computer Vision, 2008. ↑2

[45] V. Larsson and K. Åström, *Uncovering symmetries in polynomial systems*, European Conference on Computer Vision, 2016, pp. 252–267. ↑3

[46] V. Larsson, M. Oskarsson, K. Åström, A. Wallis, Z. Kukelova, and T. Pajdla, *Beyond Gröbner Bases: Basis Selection for Minimal Solvers*, 2018 IEEE Conference on Computer Vision and Pattern Recognition, CVPR 2018, Salt Lake City, UT, USA, June 18-22, 2018, 2018, pp. 3945–3954. ↑3

[47] V. Larsson, N. Zobernig, K. Taskin, and M. Pollefeys, *Calibration-free structure-from-motion with calibrated radial trifocal tensors*, European Conference on Computer Vision, 2020, pp. 382–399. ↑2, 3, 4, 7, 8, 6

[48] S. Lin and B. Sturmfels, *Polynomial relations among principal minors of a 4× 4-matrix*, Journal of Algebra **322** (2009), no. 11, 4121–4131. ↑2, 5

[49] M. Liu, C. Pradalier, and R. Siegwart, *Visual homing from scale with an uncalibrated omnidirectional camera*, IEEE Transactions on Robotics **29** (2013), no. 6, 1353–1365. ↑2

[50] E. Martyushev, J. Vráblíková, and T. Pajdla, *Optimizing elimination templates by greedy parameter search*, IEEE/CVF Conference on Computer Vision and Pattern Recognition, CVPR 2022, New Orleans, LA, USA, June 18-24, 2022, 2022, pp. 15733–15743. ↑3

[51] P. Miraldo, T. Dias, and S. Ramalingam, *A Minimal Closed-Form Solution for Multi-perspective Pose Estimation using Points and Lines*, Computer Vision - ECCV 2018 - 15th European Conference, Munich, Germany, September 8-14, 2018, Proceedings, Part XVI, 2018, pp. 490–507. ↑2

[52] P. Moulon, P. Monasse, and R. Marlet, *Global fusion of relative motions for robust, accurate and scalable structure from motion*, IEEE International Conference on Computer Vision, ICCV 2013, Sydney, Australia, December 1-8, 2013, 2013, pp. 3248–3255. ↑1

[53] T. Muir, *The relations between the coaxial minors of a determinant of the fourth order*, Transactions of The Royal Society of Edinburgh **39** (1900), no. 2, 323–339. ↑2, 5

[54] R. Mur-Artal, J. M. M. Montiel, and J. D. Tardós, *ORB-SLAM: A versatile and accurate monocular SLAM system*, IEEE Transactions on Robotics **31** (2015), no. 5, 1147–1163. ↑1

[55] E. Nanson, *On the relations between the coaxial minors of a determinant*, The London, Edinburgh, and Dublin Philosophical Magazine and Journal of Science **44** (1897), no. 269, 362–367. ↑2, 5

[56] D. Nistér, *An efficient solution to the five-point relative pose problem*, IEEE Transactions on Pattern Analysis and Machine Intelligence **26** (June 2004), no. 6, 756–770. ↑2

[57] D. Nister, R. Hartley, and H. Stewénius, *Using Galois Theory to Prove Structure from Motion Algorithms are Optimal*, 2007 IEEE Conference on Computer Vision and Pattern Recognition, 2007, pp. 1–8. ↑3, 2

[58] D. Nistér, *An efficient solution to the five-point relative pose problem*, IEEE Transactions on Pattern Analysis and Machine Intelligence **26** (2004), no. 6, 756–777. ↑2

[59] L. Oeding, *The quadrifocal variety*, Linear Algebra and its Applications **512** (2017), 306 –330. arxiv 1501.01266. ↑2

[60] L. Oeding, *Set-theoretic defining equations of the variety of principal minors of symmetric matrices*, Algebra and Number Theory **5** (2011), no. 1, 75–109. MR2833786 ↑5

[61] L. Oeding and S. V. Sam, *Equations for the fifth secant variety of Segre products of projective spaces*, Experimental Mathematics **25** (2016), no. 1, 94–99. MR3424836 ↑4

[62] C. Olsson and O. Enqvist, *Stable structure from motion for unordered image collections*, Scandinavian Conference on Image Analysis, 2011. ↑8, 7

[63] C. Olsson, V. Larsson, and F. Kahl, *A quasiconvex formulation for radial cameras*, IEEE conference on computer vision and pattern recognition, CVPR 2021, virtual, june 19-25, 2021, 2021, pp. 14576–14585. ↑3

[64] J. Pritts, Z. Kukelova, V. Larsson, Y. Lochman, and O. Chum, *Minimal solvers for rectifying from radially-distorted scales and change of scales*, International Journal of Computer Vision **128** (2020), no. 4, 950–968. ↑2

[65] L. Quan, *Two-Way Ambiguity in 2D Projective Reconstruction from Three Uncalibrated 1D Images*, IEEE Transactions on Pattern Analysis and Machine Intelligence **23** (2001), no. 2, 212–216. ↑2, 4

[66] L. Quan and T. Kanade, *Affine structure from line correspondences with uncalibrated affine cameras*, IEEE Transactions on Pattern Analysis and Machine Intelligence **19** (1997), no. 8, 834–845. ↑2

[67] R. Raguram, O. Chum, M. Pollefeys, J. Matas, and J. -M. Frahm, *USAC: A universal framework for random sample consensus*, IEEE Transactions on Pattern Analysis Machine Intelligence **35** (2013), no. 8, 2022–2038. ↑3

[68] S. Ramalingam and P. F. Sturm, *Minimal Solutions for Generic Imaging Models*, CVPR – IEEE Conference on Computer Vision and Pattern Recognition, 2008. ↑2

[69] C. Sagüés, A. C. Murillo, J. J. Guerrero, T. Goedemé, T. Tuytelaars, and L. V. Gool, *Localization with omnidirectional images using the radial trifocal tensor*, Proceedings of the 2006 IEEE International Conference on Robotics and Automation, ICRA 2006, May 15-19, 2006, Orlando, Florida, USA, 2006, pp. 551–556. ↑2

[70] J. L. Schönberger and J.-M. Frahm, *Structure-from-motion revisited*, Conference on Computer Vision and Pattern Recognition (CVPR), 2016. ↑1

[71] T. Schops, J. L. Schonberger, S. Galliani, T. Sattler, K. Schindler, M. Pollefeys, and A. Geiger, *A Multi-View Stereo Benchmark With High-Resolution Images and Multi-Camera Videos*, Proceedings IEEE Conference on Computer Vision and Pattern Recognition (CVPR) 2017, 2017. ↑7, 8, 6

[72] A. Shashua and L. Wolf, *On the structure and properties of the quadrifocal tensor*, Computer Vision - ECCV 2000, 2000, pp. 710–724 (English). ↑2

[73] A. J. Sommese and C. W. Wampler II, *The numerical solution of systems of polynomials arising in engineering and science*, World Scientific, Hackensack, NJ, 2005. MR2160078 ↑3, 6

[74] F. Sottile and T. Yahl, *Galois groups in enumerative geometry and applications*, arXiv, 2021. ↑2

[75] S. Thirthala and M. Pollefeys, *Radial multi-focal tensors*, International Journal of Computer Vision **96** (2012), no. 2, 195–211 (English). ↑2, 3

[76] S. Thirthala and M. Pollefeys, *The Radial Trifocal tensor: a Tool for Calibrating the Radial Distortion of Wide-Angle Cameras*, 2005 IEEE Computer Society Conference on Computer Vision and Pattern recognition (CVPR 2005), 20-26 June 2005, San Diego, CA, USA, 2005, pp. 321–328. ↑2

[77] B. Triggs, *Autocalibration and the absolute quadric*, Proceedings of IEEE Computer Society Conference on Computer Vision and Pattern Recognition, 1997, pp. 609–614. ↑4

[78] R. Y. Tsai, *A versatile camera calibration technique for high-accuracy 3D machine vision metrology using off-the-shelf TV cameras and lenses*, IEEE Journal on Robotics and Automation **3** (1987), no. 4, 323–344. ↑2

[79] J. Ventura, C. Arth, and V. Lepetit, *An efficient minimal solution for multi-camera motion*, Proceedings of the IEEE International Conference on Computer Vision (ICCV), 2015, pp. 747–755. ↑2